RSC Advances

PAPER

View Article Online
View Journal | View Issue

Cite this: *RSC Adv.*, 2026, **16**, 488

[BMIM]OAc promoted one-pot synthesis of pyrazolo[4′,3′:5,6]pyrido[2,3-*d*]pyrimidin-5-ones and their antimicrobial activity

Savan S. Bhalodiya, [a] Mehul P. Parmar, [a] Shana Balachandran, [b] Chirag D. Patel, [a] Arijit Nandi, [cd] Anwesha Das, [ce] Madan Kumar Arumugam [b] and Hitendra M. Patel *[a]

Received 10th December 2025
Accepted 17th December 2025

DOI: 10.1039/d5ra09581f

rsc.li/rsc-advances

A one-pot method was developed for synthesizing pyrazolo[4′,3′:5,6]pyrido[2,3-*d*]pyrimidin-5-ones using the recyclable ionic liquid catalyst [BMIM]OAc in ethanol under reflux conditions. This approach achieved high yields (76–95%) across various substrates along with straightforward product isolation and catalyst recyclability. The synthesized compounds **4(a–l)** were tested for antimicrobial activity against Gram-positive and Gram-negative bacteria, and fungal strains. Notably, compounds **4c** and **4e** showed strong antibacterial effects against *S. aureus* (MIC: 8 μg mL^{-1}), while **4a**, **4b**, and **4f** effectively inhibited *E. coli* (MIC: 8 μg mL^{-1}). Compound **4l** exhibited notable antifungal activity against *C. albicans* (MIC: 8 μg mL^{-1}), outperforming the standard drugs. Cytotoxicity assessment on HEK293 cells revealed low toxicity in most derivatives (IC_{50} > 50 μM), with halogenated analogs (**4c**, **4e**) displaying moderate activity but remaining less toxic than doxorubicin. Molecular docking and dynamics simulations confirmed stable interactions of key compounds (**4c**, **4e**, **4f**) with bacterial Tet repressor class D and fungal sterol 14-α demethylase, consistent with experimental data. Overall, this ionic liquid-catalyzed approach provides an efficient route to bioactive heterocycles with promising antimicrobial and anticancer potential.

1 Introduction

Heterocyclic structures are crucial in drug discovery, appearing in over 70% of small-molecule drugs approved in recent decades due to their ability to finely adjust properties like lipophilicity, polarity, hydrogen bonding, and ADME profiles.[1–4] Synthetic advances have enabled access to a wide variety of these compounds, speeding up medicinal chemistry efforts.[5] Fused heterocycles, for example, pyrazolo-pyrimidines, are highly regarded as privileged scaffolds because their rigid, nucleobase-like forms enhance selective binding to ATP-binding enzymes.[6–8] Multicomponent reactions (MCRs) are highly valuable in modern synthetic chemistry due to their efficiency, sustainability, and versatility in constructing complex molecules in a single step.[9–13] These reactions adhere to green chemistry principles by often removing the necessity for intermediate purification and minimizing reagent consumption.[14–17] MCRs have broad applications across pharmaceuticals, materials science, and agrochemicals, serving as a robust platform to generate extensive libraries of bioactive compounds, functional materials, and innovative molecular architectures critical for both research progress and industrial use.[18–20]

Recently, ionic liquids have become prominent catalysts in the synthesis of heterocyclic structures due to their dual role as green solvents and catalysts.[21,22] Ionic liquids act green and sustainable catalyst and solvent, the cation and anion combination can be changed for specific reaction conditions, enhances reaction efficiency.[23] Numerous one-pot MCRs conducted in ionic liquids have been reported for synthesizing diverse heterocycles such as pyrimidine, quinoline, quinazoline, pyrimido-quinoline, and pyrido-pyrimidine derivatives.[24–27] Pyrazolo, pyridine, and pyrimidine scaffolds possess various biological activity because of producing nitrogen-rich, planar frameworks capable of hydrogen bonding and π–π interactions at biomolecular sites.[28–30] Owing to these features, they are considered privileged scaffolds in medicinal

[a]*Department of Chemistry, Sardar Patel University, Vallabh Vidyanagar, Near University Circle, Vallabh Vidyanagar-388120, Gujarat, India. E-mail: hm_patel@spuvvn.edu; sa1bhalodiya@gmail.com; mpparmar1997@gmail.com; chiragkumarp23@gmail.com*

[b]*Cancer Biology Lab, Center for Molecular and Nanomedical Sciences, Sathyabama Institute of Science and Technology, Chennai-600119, Tamil Nadu, India. E-mail: shanabalachandran@gmail.com; madankumar@sathyabama.ac.in; madankumarbio@gmail.com*

[c]*Department of Pharmacy, Sanaka Educational Trust Group of Institutions (SETGOI), Durgapur, West Bengal, 713212, India. E-mail: arijitnandi57@gmail.com; dasanwesha.096@gmail.com*

[d]*Institute for Molecular Bioscience, The University of Queensland, Brisbane, 4072, Australia*

[e]*School of Pharmacy and Pharmaceutical Sciences, The University of Queensland, Brisbane, Queensland 4072 Queensland, Australia*

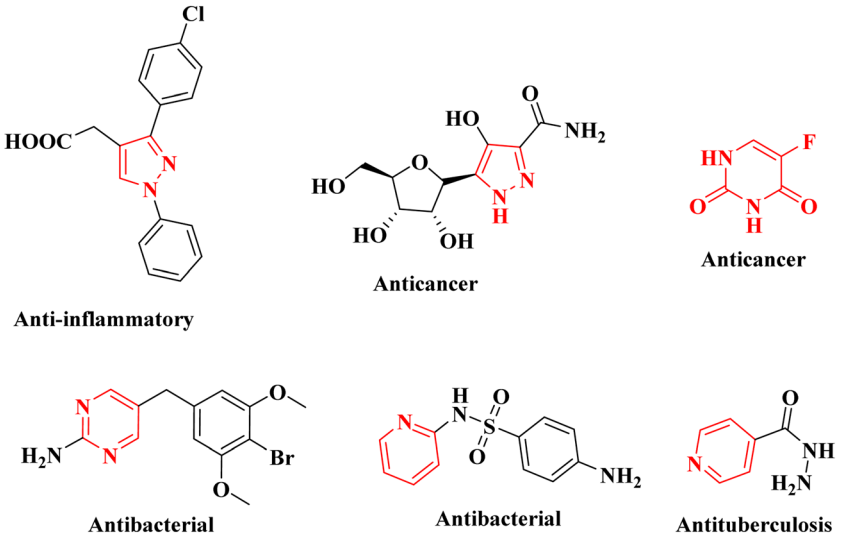

Fig. 1 Pyrazolo, pyridine nucleus-bearing drugs.

chemistry and have yielded diverse bioactive compounds, into clinical studies.[6,31,32] These heterocycles exhibit antimicrobial, antifungal, anti-inflammatory, and anticancer activities supported by SAR studies.[33–37] Such versatility underscores their potential for further development as antimicrobial agents. Some of the marketed drugs bearing pyrazole, pyridine, and pyrimidine scaffold were shown in Fig. 1.

According to literature, the rational design of the target molecules was guided by established SAR trends of barbituric and thiobarbituric derivatives. Replacement of the carbonyl oxygen with sulphur at C-2 increases lipophilicity and polarizability, enhancing passive membrane diffusion and soft–soft interactions with biological targets compared to the parent oxygen analogues.[38] Published studies report superior antibacterial profiles for thiobarbiturates *versus* barbiturates, attributed to altered hydrogen-bonding geometry and improved intracellular accumulation. Additionally, N-alkyl substitution modulates lipophilicity and steric bulk; ethyl chains provide an optimal balance between hydrophobicity and solubility, improving bacterial membrane penetration relative to methyl substituents. Therefore, systematic incorporation of the C=S group and variation of N-alkyl chain length (methyl *vs.* ethyl) was selected to evaluate how physicochemical changes translate into antimicrobial potency.[39,40]

Several protocols exist for constructing pyrazolo-pyrido-pyrimidine scaffolds by employing various catalyst like *p*-TSA,[41] cellulose supported acidic ionic liquid,[42] (Na{[Nd (pydc-OH)$(H_2O)_4$]$_3$}[$SiW_{12}O_{40}$]),[43] ZIF-8@GO@$MgFe_2O_4$,[44] Nano-ZnO,[45] triethyl amine,[46] conditions. To the best of our knowledge, there is a lack of alternative methodologies for synthesizing pyrazolo-pyrido-pyrimidine scaffolds has been reported in the current literature. Therefore, exploring new and diverse strategies for their synthesis remains essential due to their significant importance.

To the best of our knowledge, this is the first report describing a recyclable ionic-liquid-promoted one-pot MCR synthesis of pyrazolo[4′,3′:5,6]pyrido[2,3-*d*]pyrimidin-5-ones. Compared with previously published protocols employing different catalysts, the present methodology offers several distinctive advantages, including milder reaction conditions, significantly higher yields, short reaction time, simple product isolation, and efficient catalyst recyclability. Furthermore, the current work not only provides an environmentally sustainable synthetic route but also delivers biologically active compounds with promising antimicrobial profiles, thereby demonstrating practical medicinal relevance (Scheme 1).

2 Experimental

2.1 Synthetic protocol for pyrazolo[4′,3′:5,6]pyrido[2,3-*d*] pyrimidin-5-ones 4(a–l)

Using 10 mol% [BMIM]OAc as the catalyst, compounds **4(a–l)** were synthesized by reacting 5-amino-3-methyl-1-phenylpyrazole (**1**, 1.0 mmol), 1,3-diethylthiobarbituric acid (**2**, 1.0 mmol), and the corresponding aromatic aldehydes (**3(a–l)**, 1.0 mmol) in ethanol under reflux conditions. The progress of the reaction was monitored by thin-layer chromatography (TLC) using silica gel 60 F254 plates with an ethyl acetate/hexane (3 : 7, v/v) solvent system. After reaction completion, the mixture was allowed to cool to room temperature, during which a solid product precipitated in the reaction flask. The reaction mixture was then quenched by the addition of water. The resulting solid was collected by filtration and washed thoroughly with small amounts of ethanol followed by hot water to afford the pure product.

2.2 Analytical data of synthesized compounds 4(a–l)

2.2.1 4-(4-chlorophenyl)-3,6,8-trimethyl-1-phenyl-7-thioxo-1,4,6,7,8,9-hexahydro-5*H*-pyrazolo[4′,3′:5,6]pyrido[2,3-*d*] pyrimidin-5-one 4a. Yellow solid; M.P.: >200 °C; IR (KBr, cm^{-1}): 3173 (m, N–H), 1705 (s, C=O), 1137 (s, C=S) ^{1}H NMR (400 MHz, DMSO-d_6) δ: 9.42 (s, 1H, N–H), 7.32 (d, 2H, $J = 4$ Hz, Ar–H),

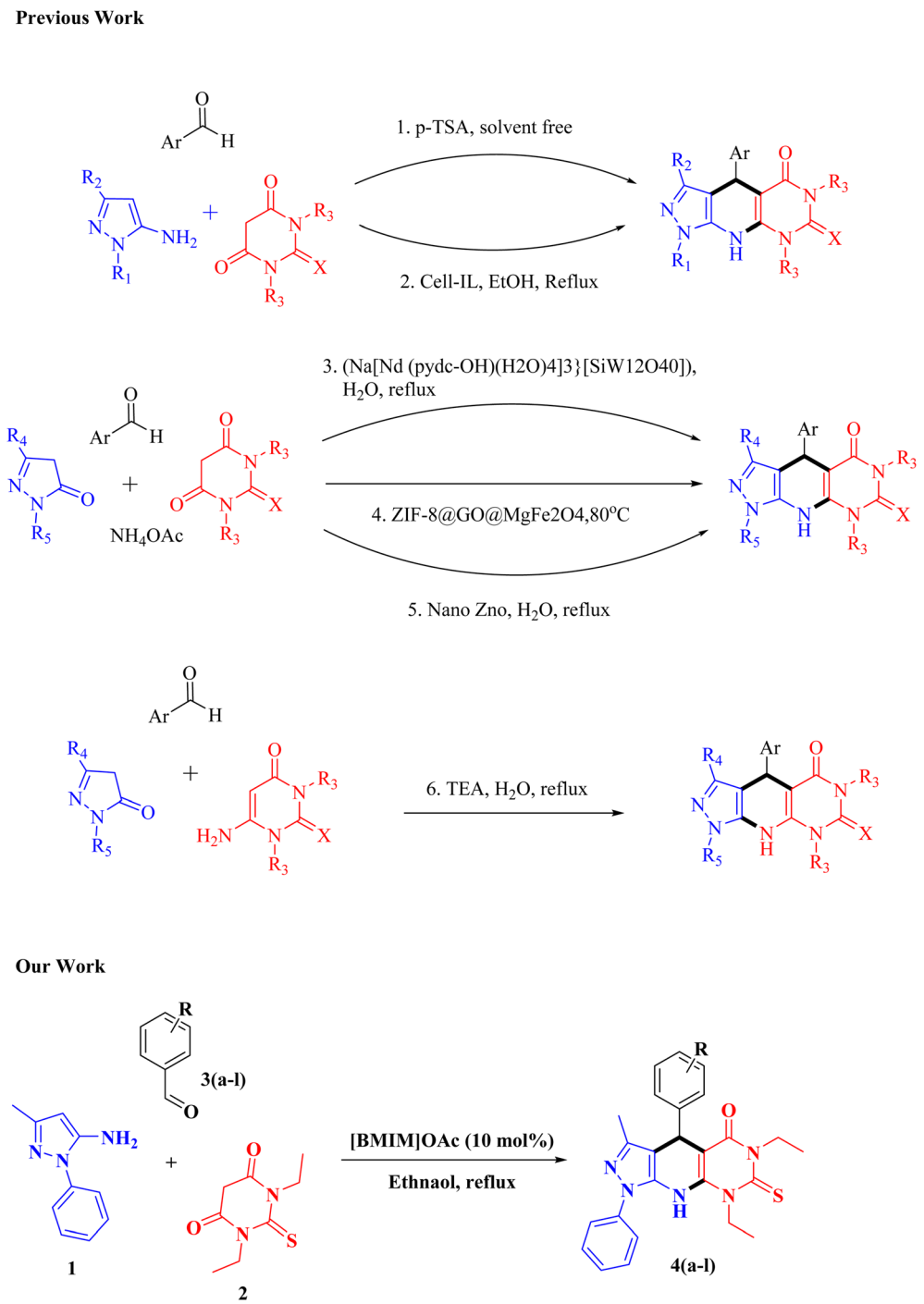

Scheme 1 Reaction protocols of pyrazolo-pyrido-pyrimidine scaffolds.

7.08 (d, 2H, J = 8 Hz, Ar–H), 6.95 (s, 1H, Ar–H), 6.62 (t, 2H, J = 4 Hz, Ar–H), 6.53 (d, 2H, J = 4 Hz, Ar–H), 5.37 (s, 1H, C–H), 4.41 (q, 4H, J = 8 Hz, CH_2), 2.07 (s, 3H, CH_3), 1.30 (t, 6H, J = 8 Hz, CH_3) ^{13}C NMR (126 MHz, DMSO-d_6) δ: 171.97, 162.81, 160.82, 156.82, 152.44, 151.08, 144.83, 132.54, 131.41, 125.08, 124.24, 121.15, 115.34, 133.37, 84.89, 47.28, 43.63, 17.19, 13.11, 12.04. Molecular weight: 461.95, MS(ESI m/z): 462.82.

2.2.2 4-(4-bromophenyl)-6,8-diethyl-3-methyl-1-phenyl-7-thioxo-1,4,6,7,8,9-hexahydro-5*H*-pyrazolo[4′,3′:5,6]pyrido[2,3-*d*] pyrimidin-5-one 4b. Yellow solid; M.P.: >200 °C; IR (KBr, cm^{-1}): 3168 (m, N–H), 1712 (s, C=O), 1134 (s, C=S) ^{1}H NMR (400 MHz, DMSO-d_6) δ: 9.86 (s, 1H, N–H), 7.62 (t, 1H, J = 8 Hz, Ar–H), 7.51 (d, 2H, J = 8 Hz, Ar–H), 7.45 (d, 2H, J = 4 Hz, Ar–H), 7.36 (d, 2H, J = 8 Hz, Ar–H), 7.18 (d, 2H, J = 8 Hz, Ar–H), 5.51 (s, 1H, C–H), 4.42 (q, 4H, J = 8 Hz, CH_2), 2.12 (s, 3H, CH_3), 1.46 (t, 6H, J = 8 Hz, CH_3) ^{13}C NMR (126 MHz, DMSO-d_6) δ: 174.36, 167.85, 161.17, 145.70, 142.78, 140.57, 138.11, 135.76, 133.37, 129.99,

129.44, 128.61., 127.54, 125.60, 85.90, 47.31, 43.92, 43.07. Molecular weight: 506.40, MS(ESI *m*/*z*): 507.37.

2.2.3 6,8-Diethyl-4-(4-fluorophenyl)-3-methyl-1-phenyl-7-thioxo-1,4,6,7,8,9-hexahydro-5*H*-pyrazolo[4′,3′:5,6]pyrido[2,3-*d*] pyrimidin-5-one 4c. Yellow solid; M.P.: >200 °C; IR (KBr, cm^{-1}): 3127 (m, N–H), 1717 (s, C=O), 1121 (s, C=S) ^{1}H NMR (400 MHz, DMSO-d_6) δ: 9.89 (s, 1H, N–H), 7.61 (t, 2H, J = 8 Hz, Ar–H), 7.52 (d, 2H, J = 8 Hz, Ar–H), 7.46 (q, 2H, J = 8 Hz, Ar–H), 7.36 (d, 2H, J = 8 Hz, Ar–H), 7.11 (s, 1H, Ar–H), 5.56 (s, 1H, C–H), 4.40 (q, 4H, J = 8 Hz, CH_2), 2.10 (s, 3H, CH_3), 1.43 (t, 6H, J = 8 Hz, CH_3) ^{13}C NMR (126 MHz, DMSO-d_6) δ: 171.51, 163.13, 160.09, 140.27, 139.00, 136.86, 134.45, 132.11, 130.06, 129.70, 127.03, 122.42, 114.03, 112.99, 82.23, 48.42, 42.68, 42.13, 17.84, 12.25, 11.58. Molecular weight: 445.50, MS(ESI *m*/*z*): 444.83.

2.2.4 6,8-Diethyl-3-methyl-4-(4-nitrophenyl)-1-phenyl-7-thioxo-1,4,6,7,8,9-hexahydro-5*H*-pyrazolo[4′,3′:5,6]pyrido[2,3-*d*] pyrimidin-5-one 4d. Yellow solid; M.P.: >200 °C; IR (KBr, cm^{-1}): 3176 (m, N–H), 1723 (s, C=O), 1532 (s, NO_2), 1364 (s, NO_2), 1127 (s, C=S) ^{1}H NMR (400 MHz, DMSO-d_6) δ: 9.94 (s, 1H, N–H), 7.63 (t, 2H, J = 8 Hz, Ar–H), 7.48 (m, 3H, Ar–H), 7.38 (d, 2H, J = 4 Hz, Ar–H), 3.32 (t, 2H, J = 8 Hz, Ar–H), 5.66 (s, 1H, C–H), 4.45 (q, 4H, J = 8 Hz, CH_2), 2.06 (s, 3H, CH_3), 1.35 (t, 6H, J = 8 Hz, CH_3) ^{13}C NMR (126 MHz, DMSO-d_6) δ: 173.44, 167.21, 164.63, 144.57, 143.24, 141.77, 139.98, 138.55, 136.11, 133.96, 131.72, 130.00, 127.87, 116.93, 83.37, 48.11, 42.90, 42.15, 18.05, 12.68, 11.80. Molecular weight: 472.51, MS(ESI *m*/*z*): 471.29.

2.2.5 4-(3-Chlorophenyl)-6,8-diethyl-3-methyl-1-phenyl-7-thioxo-1,4,6,7,8,9-hexahydro-5*H*-pyrazolo[4′,3′:5,6]pyrido[2,3-*d*] pyrimidin-5-one 4e. Yellow solid; M.P.: >200 °C; IR (KBr, cm^{-1}): 3165 (m, N–H), 1719 (s, C=O), 1113 (s, C=S) ^{1}H NMR (400 MHz, DMSO-d_6) δ: 9.66 (s, 1H, N–H), 7.57 (s, 1H, Ar–H), 7.55 (s, 1H, Ar–H), 7.53 (d, 5H, J = 4 Hz, Ar–H), 7.40 (t, 2H, J = 4 Hz, Ar–H), 5.38 (s, 1H, C–H), 4.43 (q, 4H, J = 8 Hz, CH_2), 2.14 (s, 3H, CH_3), 1.40 (t, 6H, J = 8 Hz, CH_3) ^{13}C NMR (126 MHz, DMSO-d_6) δ: 171.99, 165.88, 163.23, 145.43, 143.36, 141.09, 139.04, 135.48, 133.49, 131.91, 129.03, 124.81, 122.64, 120.02, 117.15, 112.48, 84.36, 49.47, 43.74, 42.72, 18.35, 13.06, 12.18. Molecular weight: 461.95, MS(ESI *m*/*z*): 460.38.

2.2.6 4-(3-Bromophenyl)-6,8-diethyl-3-methyl-1-phenyl-7-thioxo-1,4,6,7,8,9-hexahydro-5*H*-pyrazolo[4′,3′:5,6]pyrido[2,3-*d*] pyrimidin-5-one 4f. Yellow solid; M.P.: >200 °C; IR (KBr, cm^{-1}): 3159 (m, N–H), 1725 (s, C=O), 1129 (s, C=S) ^{1}H NMR (400 MHz, DMSO-d_6) δ: 9.44 (s, 1H, N–H), 7.34 (d, 2H, J = 8 Hz, Ar–H), 7.12 (t, 3H, J = 8 Hz, Ar–H), 6.88 (d, 2H, J = 4 Hz, Ar–H), 6.57 (d, 2H, J = 4 Hz, Ar–H), 5.41 (s, 1H, C–H), 4.40 (q, 4H, J = 8 Hz, CH_2), 2.10 (s, 3H, CH_3), 1.37 (t, 6H, J = 8 Hz, CH_3); ^{13}C NMR (126 MHz, DMSO-d_6) δ: 173.73, 167.90, 165.84, 144.05, 141.82, 139.53, 139.16, 135.50, 133.21, 131.04, 129.11, 127.35, 122.82, 122.02, 119.80, 117.25, 83.84, 47.80, 43.21, 42.59, 18.93, 12.74, 11.77. Molecular weight: 506.40, MS(ESI *m*/*z*): 507.57.

2.2.7 6,8-Diethyl-4-(3-fluorophenyl)-3-methyl-1-phenyl-7-thioxo-1,4,6,7,8,9-hexahydro-5*H*-pyrazolo[4′,3′:5,6]pyrido[2,3-*d*] pyrimidin-5-one 4g. Yellow solid; M.P.: >200 °C; IR (KBr, cm^{-1}): 3173 (m, N–H), 1708 (s, C=O), 1136 (s, C=S) ^{1}H NMR (400 MHz, DMSO-d_6) δ: 9.51 (s, 1H, N–H), 8.20 (d, 3H, J = 4 Hz, Ar–H), 8.07 (t, 2H, J = 2 Hz, Ar–H), 7.88 (t, 2H, J = 4 Hz, Ar–H), 6.63 (q, 2H, J = 4 Hz, Ar–H), 5.50 (s, 1H, C–H), 4.49 (q, 4H, J = 8 Hz, CH_2), 2.05 (s, 3H, CH_3), 1.30 (t, 6H, J = 8 Hz, CH_3) ^{13}C NMR (126 MHz, DMSO-d_6) δ: 173.45, 167.16, 165.79, 144.47, 142.57, 139.21, 137.30, 135.17, 131.50, 128.27, 123.63, 121.23, 119.07, 116.59, 114.43, 114.28, 83.22, 43.30, 42.29, 18.32, 12.58, 11.67. Molecular weight: 445.50, MS(ESI *m*/*z*): 444.92.

2.2.8 6,8-Diethyl-3-methyl-4-(3-nitrophenyl)-1-phenyl-7-thioxo-1,4,6,7,8,9-hexahydro-5*H*-pyrazolo[4′,3′:5,6]pyrido[2,3-*d*] pyrimidin-5-one 4h. Yellow solid; M.P.: >200 °C; IR (KBr, cm^{-1}): 3179 (m, N–H), 1711 (s, C=O), 1521 (s, NO_2), 1352 (s, NO_2), 1135 (s, C=S) ^{1}H NMR (400 MHz, DMSO-d_6) δ: 9.52 (s, 1H, N–H), 7.64 (d, 3H, J = 4 Hz, Ar–H), 7.59 (d, 1H, J = 4 Hz, Ar–H), 7.26 (d, 3H, J = 8 Hz, Ar–H), 7.12 (t, 2H, J = 8 Hz, Ar–H), 5.55 (s, 1H, C–H), 4.37 (q, 4H, J = 8 Hz, CH_2), 2.09 (s, 3H, CH_3), 1.13 (t, 6H, J = 8 Hz, CH_3) ^{13}C NMR (126 MHz, DMSO-d_6) δ: 174.69, 163.38, 159.76, 144.57, 137.87, 135.78, 131.68, 130.26, 130.02, 128.70, 128.18, 126.49, 125.31, 123.50, 122.70, 117.14, 116.65, 83.84, 48.46, 43.20, 42.38, 18.53, 12.81, 12.13. Molecular weight: 472.51, MS(ESI *m*/*z*): 471.08.

2.2.9 4-(2-Chlorophenyl)-6,8-diethyl-3-methyl-1-phenyl-7-thioxo-1,4,6,7,8,9-hexahydro-5*H*-pyrazolo[4′,3′:5,6]pyrido[2,3-*d*] pyrimidin-5-one 4i. Yellow solid; M.P.: >200 °C; IR (KBr, cm^{-1}): 3164 (m, N–H), 1709 (s, C=O), 1127 (s, C=S) ^{1}H NMR (400 MHz, DMSO-d_6) δ: 9.63 (s, 1H, N–H), 7.44 (d, 3H, J = 4 Hz, Ar–H), 7.39 (q, 1H, J = 4 Hz, Ar–H), 7.07 (d, 2H, J = 8Hz, Ar–H), 7.79 (d, 2H, J = 8 Hz, Ar–H), 6.53 (q, 1H, J = 4 Hz, Ar–H), 5.35 (s, 1H, C–H), 4.46 (q, 4H, J = 8 Hz, CH_2), 2.08 (s, 3H, CH_3), 1.33 (t, 6H, J = 8 Hz, CH_3) ^{13}C NMR (126 MHz, DMSO-d_6) δ: 174.73, 165.43, 161.45, 144.89, 142.11, 137.22, 135.59, 133.88, 131.72, 128.79, 125.85, 123.76, 121.64, 120.27, 116.63, 115.18, 83.45, 48.81, 43.36, 42.49, 18.09, 12.64, 11.89. Molecular weight: 461.95, MS(ESI *m*/*z*): 460.92.

2.2.10 4-(2-Bromophenyl)-6,8-diethyl-3-methyl-1-phenyl-7-thioxo-1,4,6,7,8,9-hexahydro-5*H*-pyrazolo[4′,3′:5,6]pyrido[2,3-*d*] pyrimidin-5-one 4j. Yellow solid; M.P.: >200 °C; IR (KBr, cm^{-1}): 3172 (m, N–H), 1718 (s, C=O), 1131 (s, C=S) ^{1}H NMR (400 MHz, DMSO-d_6) δ: 9.74 (s, 1H, N–H), 7.43 (d, 1H, J = 8 Hz, Ar–H), 7.39 (s, 1H, Ar–H), 7.16 (q, 2H, J = 4 Hz, Ar–H), 7.10 (d, 2H, J = 8 Hz, Ar–H), 6.89 (d, 2H, J = 8 Hz, Ar–H), 6.80 (s, 1H, Ar–H), 5.34 (s, 1H, C–H), 4.41 (q, 4H, J = 8 Hz, CH_2), 2.05 (s, 3H, CH_3), 1.32 (t, 6H, J = 8 Hz, CH_3) ^{13}C NMR (126 MHz, DMSO-d_6) δ: 173.87, 164.47, 162.16, 144.52, 143.08, 139.83, 137.21, 134.47, 130.55, 129.65, 128.86, 125.68, 123.58, 121.59, 118.51, 116.67, 84.33, 49.02, 43.56, 42.93, 18.81, 12.80, 11.95. Molecular weight: 506.40, MS(ESI *m*/*z*): 507.62.

2.2.11 6,8-Diethyl-3-methyl-1-phenyl-7-thioxo-4-(4-(trifluoromethyl)phenyl)-1,4,6,7,8,9-hexahydro-5*H*-pyrazolo [4′,3′:5,6]pyrido[2,3-*d*]pyrimidin-5-one 4k. Yellow solid; M.P.: >200 °C; IR (KBr, cm^{-1}): 3172 (m, N–H), 1713 (s, C=O), 1129 (s, C=S); ^{1}H NMR (500 MHz, DMSO-d_6) δ: 9.82 (s, 1H, N–H), 7.45 (d, 2H, J = 8 Hz, Ar–H), 7.26 (d, 2H, J = 8 Hz, Ar–H), 7.11 (m, 4H, Ar–H), 6.87 (d, 1H, J = 4Hz, Ar–H), 5.47 (s, 1H, C–H), 4.39 (q, 4H, J = 8 Hz, CH_2), 2.08 (s, 3H, CH_3), 1.31 (t, 6H, J = 8 Hz, CH_3) ^{13}C NMR (126 MHz, DMSO-d_6) δ: 173.06, 163.93, 161.61, 143.60, 142.11, 136.99, 135.31, 133.44, 131.46, 128.41, 123.55, 122.61, 117.37, 116.73, 83.80, 49.23, 43.46, 42.63, 18.89, 12.38, 11.35. Molecular weight: 495.51, MS(ESI *m*/*z*): 496.56.

2.2.12 4-(6,8-Diethyl-3-methyl-5-oxo-1-phenyl-7-thioxo-4,5,6,7,8,9-hexahydro-1*H*-pyrazolo[4′,3′:5,6]pyrido[2,3-*d*]pyrimidin-4-yl)benzonitrile 4l. Yellow solid; M.P.: >200 °C; IR (KBr, cm^{-1}): 3177 (m, N–H), 2242 (s, CN), 1715 (s, C═O), 1131 (s, C═S) ^{1}H NMR (500 MHz, DMSO-d_6) δ: 9.89 (s, 1H, N–H), 7.61 (t, 2H, J = 8 Hz, Ar–H), 7.52 (d, 2H, J = 8 Hz, Ar–H), 7.46 (q, 2H, J = 8 Hz, Ar–H), 7.36 (d, 2H, J = 8 Hz, Ar–H), 7.11 (s, 1H, Ar–H), 5.56 (s, 1H, C–H), 4.42 (q, 4H, J = 8 Hz, CH_2), 2.10 (s, 3H, CH_3), 1.43 (t, 6H, J = 8 Hz, CH_3) ^{13}C NMR (126 MHz, DMSO-d_6) δ: 175.04, 167.36, 165.50, 143.71, 143.28, 137.62, 132.56, 131.65, 131.59, 128.35, 123.61, 122.79, 117.37, 116.78, 85.35, 50.17, 44.60, 43.37, 19.20, 14.25, 13.38. Molecular weight: 452.52, MS(ESI m/z): 453.570.

2.3 Biological screening

2.3.1 Antimicrobial assay. The antimicrobial activity of compounds **4(a–l)** was assessed using the broth microdilution method consistent with our established protocols. Standard Gram-positive bacteria (*Staphylococcus aureus*, *Bacillus subtilis*) and Gram-negative bacteria (*Escherichia coli*) were used for antibacterial studies, while antifungal activity was evaluated against *Candida albicans* and *Aspergillus niger*. Stock solutions (1 mg mL^{-1}) of each compound were prepared in DMSO and diluted two-fold to obtain final test concentrations ranging from 1 to 512 μg mL^{-1} in Mueller–Hinton Broth (MHB) for bacteria and RPMI-1640 medium for fungi. Each well of a 96-well plate received 100 μL of inoculum (~5 × 10^5 CFU mL^{-1}) and 100 μL of compound dilution. Plates were incubated at 37 °C for 18–24 h (bacteria) or 28–30 °C for 48 h (fungi). The minimum inhibitory concentration (MIC) was calculated as the lowest concentration showing no visible turbidity. Tetracycline and chloramphenicol (bacteria) and fluconazole and miconazole (fungi) served as positive controls; DMSO (≤1%) served as vehicle control. All experiments were performed in triplicate.

2.3.2 Cytotoxicity assay. The cytotoxic potential of **4(a–l)** was evaluated on HEK-293 human embryonic kidney cells. Cells were cultured in DMEM supplemented with 10% fetal bovine serum and 1% penicillin–streptomycin at 37 °C in 5% CO_2. For the assay, cells (5 × 10^3 per well) were seeded in 96-well plates and allowed to adhere overnight. Serial dilutions of each compound (0.1–100 μM) were added and incubated for 48 h. MTT reagent (0.5 mg mL^{-1}) was then added and incubated for 4 h; the resulting formazan crystals were dissolved in DMSO, and absorbance was read at 570 nm. Cell viability (%) was calculated relative to control and IC_{50} values determined using nonlinear regression. Doxorubicin served as positive control. All assays were performed in triplicate, and results were expressed as Mean ± SEM. The HEK 293 human embryonic kidney cells were procured from National centre for cell sciences (NCCS),

Table 1 Optimized reaction circumstances for synthesis of pyrazolo[4′,3′:5,6]pyrido[2,3-*d*]pyrimidin-5-one **4a**[a,b]

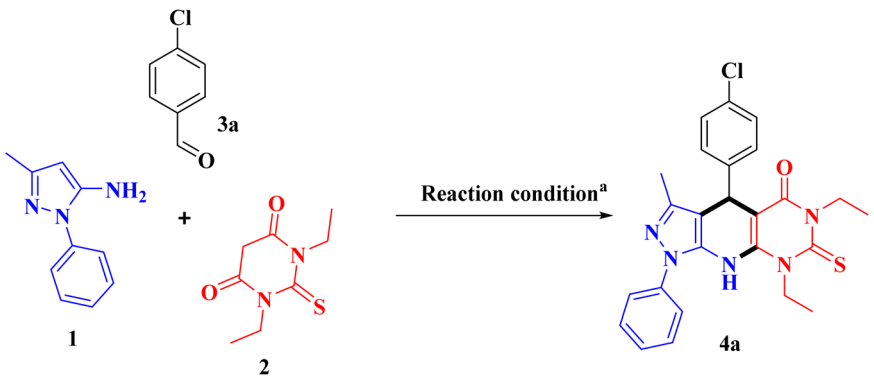

Entry	Catalyst (mol%)	Solvent	Temperature (°C)	Time (min)	Yield[b] (%)
1	—	Ethanol	Reflux	—	—
2	*p*-TSA (20)	Ethanol	Reflux	180	77
3	*p*-TSA (20)	Acetonitrile	Reflux	160	82
4	*p*-TSA (20)	*N*,*N*′-Dimethyl formamide	Reflux	160	85
5	L-Proline (20)	Ethanol	Reflux	200	68
6	L-Proline (20)	Acetonitrile	Reflux	210	59
7	—	Acetic acid	Reflux	140	80
8	[BMIM]Cl (20)	Ethanol	Reflux	120	87
9	[BMIM]Cl (10)	Ethanol	Reflux	150	75
10	[BMIM]OAc (20)	Ethanol	Reflux	90	91
11	[BMIM]OAc (15)	Ethanol	Reflux	90	90
12	[BMIM]OAc (10)	Ethanol	**Reflux**	**95**	**90**

[a] Reaction conditions: 5-amino-3-methyl-1-phenyl pyrazole **1** (1.0 mmol), 1,3-diethylthiobarbituric acid **2** (1.0 mmol), and *p*-chlorobenzaldehyde **3a** (1.0 mmol). [b] Isolated yield.

Pune, India. The cells are maintained and experiments were performed in cancer biology lab, centre for molecular and nanomedical sciences, Sathyabama Institute of Science and Technology, Chennai, India.

2.4 Molecular docking

The crystal structures of the Tet repressor class D bound to tetracycline (PDB ID: 2VKE) and the sterol 14-alpha demethylase complexed with the tetrazole-based antifungal candidate VT1161 (PDB ID: 5TZ1) were obtained from the RCSB Protein Data Bank. Both protein structures were processed using the Protein Preparation Wizard in Schrödinger (version 2017_2) 47, 48 to eliminate water molecules, reconstruct missing loops and side chains, and add hydrogen atoms for proper structural optimization. Protonation states and partial charges were assigned using the OPLS3 force field. The protein structures were subsequently subjected to restrained minimization until the root-mean-square deviation (RMSD) of non-hydrogen atoms reached 0.3 Å. Ligand preparation was carried out with the LigPrep module in the Schrödinger 2017-2 suite to generate possible tautomers and predict ionization states at pH 7.0 ± 2.0 using Epik. Receptor grids were then constructed around the co-crystallized ligand binding site of each protein's crystal structure. Finally, molecular docking was performed using the Glide XP protocol with the optimized receptor models.

2.5 MD simulations

MD simulations of the docked protein–ligand complexes were performed using the Desmond module within the Schrödinger software suite. The simulation system was constructed in an

Table 2 Substrate scopes for pyrazolo[4′,3′:5,6]pyrido[2,3-*d*]pyrimidines **4(a–l)**[a]

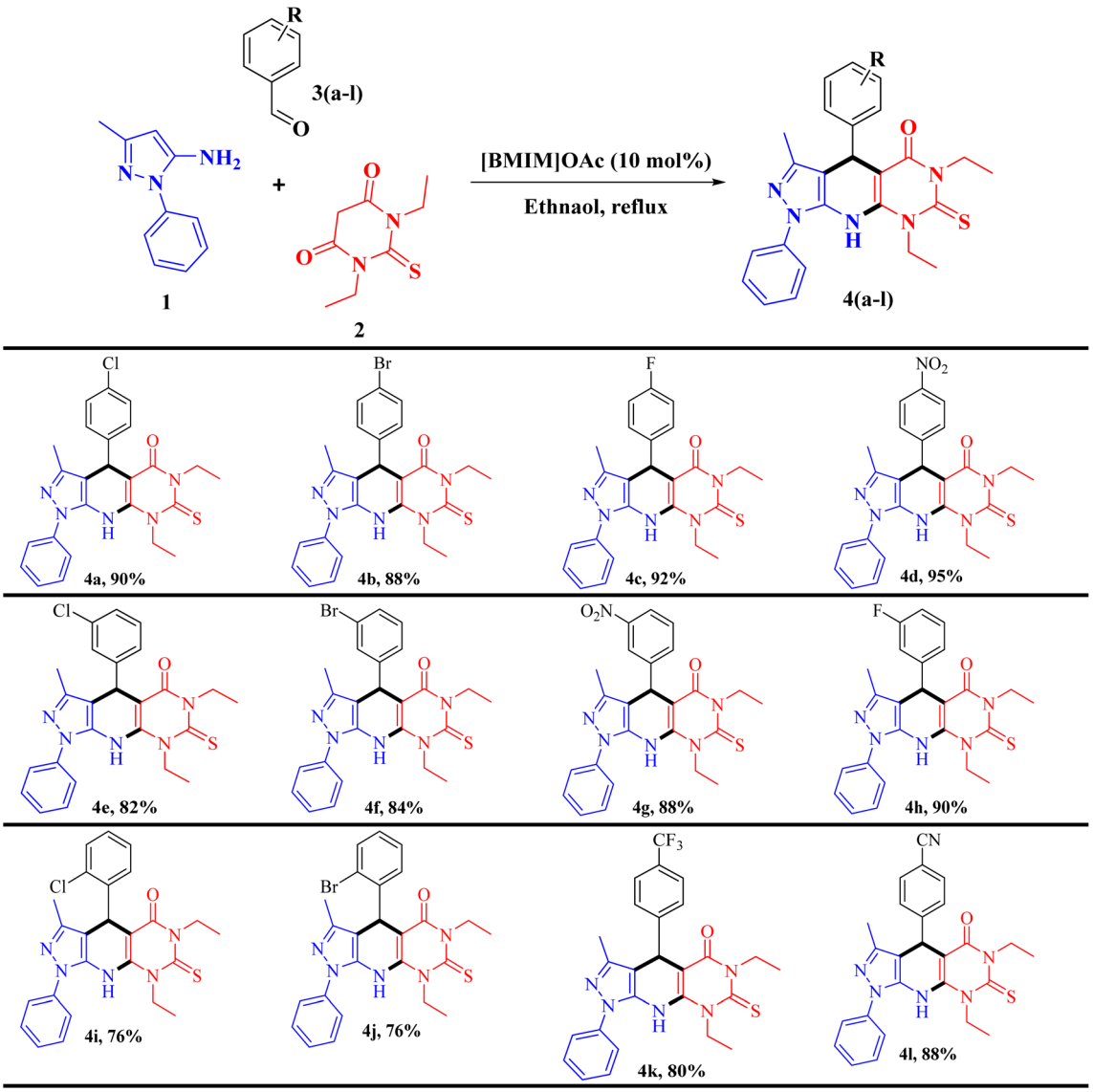

[a] Reaction conditions: 5-amino-3-methyl-1-phenyl pyrazole **1** (1.0 mmol), 1,3-diethylthiobarbituric acid **2** (1.0 mmol), and aromatic aldehyde **3(a–l)** (1.0 mmol); [BMIM]OAc (10 mol%), 4 mL ethanol, reflux.

Fig. 2 Reusability of [BMIM]OAc.

orthorhombic box *via* the System Builder panel, employing the simple point charge (SPC) model to represent water molecules. Simulations were carried out under an NPT ensemble at 310 K and 1.013 bar for a duration of 100 ns. Results from the molecular dynamics analyses were evaluated using the Simulation Interaction Diagram tool available in Desmond (The University of Queensland Research Computing Centre). 2024. Bunya supercomputer. Brisbane, Queensland, Australia. https://dx.doi.org/10.48610/wf6c-qy55).[47–49]

3 Result and discussion

3.1 Chemistry

At the beginning of our experiment, we chose 5-amino-3-methyl-1-phenyl pyrazole (**1**, 1.0 mmol), 1,3-diethylthiobarbituric acid (**2**, 1 mmol), and *p*-chlorobenzaldehyde (**3**, 1 mmol) as model substrates to react in one-pot process. To determine the optimal reaction conditions for reaction, we tested different solvents and catalysts. Our first attempt involved heating the reactants in ethanol without using any catalyst for 24 hours, but it did not result in the desired product (entry 1, Table 1). The model reaction was tested with several different catalysts, as shown in Table 1. Among these, [BMIM]OAc at (10 mol%) in ethanol

Table 4 IC_{50} values (μM) of **4(a–l)** on HEK-293 cells (mean ± SEM, $n = 3$)

Compound	IC_{50} (μM)
4a	102 ± 3.5
4b	60 ± 2.8
4c	**45 ± 2.1**
4d	55 ± 2.5
4e	**42 ± 1.9**
4f	58 ± 2.7
4g	80 ± 3.0
4h	65 ± 2.6
4i	100 ± 3.7
4j	50 ± 2.3
4k	70 ± 2.9
4l	55 ± 2.4
Doxorubicin	5 ± 0.4

Table 3 MIC values (μg mL^{-1}) of **4(a–l)** against bacteria and fungi (mean ± SEM, $n = 3$)

Compound	*S. aureus*	*B. subtilis*	*E. coli*	*C. albicans*	*A. niger*
4a	32 ± 1.5	64 ± 2.0	**8 ± 2.1**	64 ± 3.0	128 ± 3.4
4b	16 ± 1.0	32 ± 1.3	**8 ± 2.2**	32 ± 2.0	64 ± 2.5
4c	**8 ± 0.9**	**16 ± 1.1**	32 ± 1.5	32 ± 1.8	64 ± 2.0
4d	16 ± 1.2	32 ± 1.4	16 ± 1.8	32 ± 1.9	64 ± 2.3
4e	**8 ± 0.8**	**16 ± 1.0**	32 ± 1.2	32 ± 1.5	64 ± 2.1
4f	16 ± 1.3	32 ± 1.5	**8 ± 2.0**	32 ± 2.1	64 ± 2.6
4g	32 ± 1.4	32 ± 1.6	64 ± 2.3	64 ± 2.5	128 ± 3.0
4h	16 ± 1.2	32 ± 1.4	32 ± 1.9	32 ± 2.0	64 ± 2.3
4i	64 ± 2.1	64 ± 2.4	128 ± 3.2	32 ± 3.0	128 ± 3.5
4j	16 ± 1.0	32 ± 1.2	64 ± 2.0	32 ± 2.1	64 ± 2.5
4k	32 ± 1.3	32 ± 1.5	64 ± 2.1	16 ± 2.4	128 ± 3.2
4l	16 ± 1.1	32 ± 1.3	32 ± 1.8	**8 ± 2.0**	64 ± 2.2
Tetracycline	36 ± 0.02	72 ± 0.05	16 ± 0.6	—	—
Chloramphenicol	38.8 ± 0.04	88.3 ± 0.05	42.5 ± 1.6		
Fluconazole				64.0 ± 0.05	98.6 ± 0.06
Miconazole	—	—	—	126 ± 0.2	84.5 ± 0.8

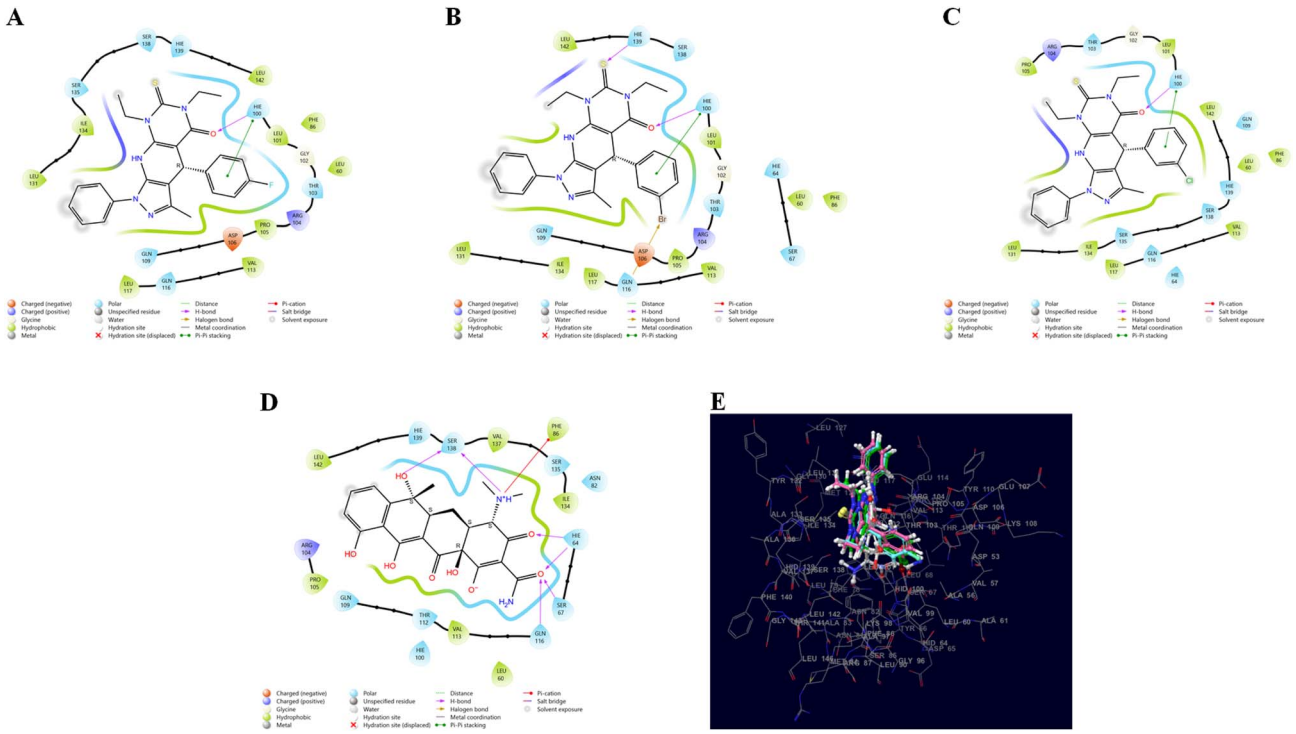

Fig. 3 (A) **4c**, (B) **4e**, (C) **4f**, and (D) tetracycline were docked into the crystal structure of Tet repressor class D (PDB ID: 2VKE) to identify potential interacting residues in the tetracycline binding site. (E) Superimposition of **4c**, **4e**, **4f**, and tetracycline in the tetracycline binding site of Tet repressor class D (PDB ID: 2VKE).

Table 5 Amino acid residues involved in interactions between the standard compounds and the experimentally identified top antibacterial and antifungal candidates with their respective targets

Compound	Docking score (kcal mol^{-1})	H-bond	Hydrophobic interaction	Polar bond
PDB ID: 2VKE				
4c	−4.378	Hie100	Leu60, Phe86, Leu101, Pro105, Val113, Leu117, Leu131, Ile134, and Leu142	Hie100, Thr103, Gln109, Gln116, Ser135, Ser138, and Hie139
4e	−4.672	Hie100	Leu60, Phe86, Leu101, Pro105, Val113, Leu117, Leu131, Ile134, and Leu142	Hie64, Hie100, Thr103, Gln109, Gln116, Ser135, Ser138, and Hie139
4f	**−4.704**	Hie100	Leu60, Phe86, Leu101, Pro105, Val113, Leu117, Leu131, Ile134, and Leu142	Hie64, Ser67, Hie100, Thr103, Gln109, Gln116, Ser138, and Hie139
Tetracycline	−5.108	—	Leu60, Phe86, Pro105, Val113, Val137, Ile134, and Leu142	Hie64, Ser67, Asn82, Hie100, Gln109, Thr112, Gln116, Ser135, Ser138, and Hie139
PDB ID: 5TZ1				
4c	−7.627	—	Phe105, Tyr118, Leu121, Phe126, Ile131, Tyr132, Leu139, Phe228, Leu300, Ile304, Leu376, Ile379, Phe463, Cys470, Ile471, Met508, and Val509	Thr122, Thr311, and His468
4e	**−7.985**	Tyr132	Leu121, Ile131, Tyr132, Leu139, Phe228, Ile304, Pro375, Leu376, Phe463, Cys470, Ile471, Phe475, Ala476, and Met508	Thr311 and His468
4f	−6.969	—	Tyr118, Leu121, Phe126, Ile131, Tyr132, Phe228, Leu300, Ile304, Leu370, Met374, Pro375, Leu376, Ile379, Pro462, Phe462, Phe463, Cys470, Ile471, Ala476, and Met508	Thr311 and His468
Fluconazole	−7.589	Tyr132	Tyr118, Leu121, Phe126, Ile131, Tyr132, Phe228, Phe233, Leu376, Ile379, Phe380, Met508, and Val509	Thr122, Thr311, and Thr378
Miconazole	−9.792	Tyr132, Cys470	Tyr118, Leu121, Phe126, Ile131, Tyr132, Leu139, Phe228, Phe233, Leu300, Ile304, Ile379, Cys470, Ile471, and Met508	Thr122, Thr122, and Thr311

worked best, leading to full conversion of the starting materials, utilizing these best conditions, we did multicomponent reactions with compound **1**, **2**, and **3(a–l)** to check how well and wide this method works. Aromatic aldehydes with electron-withdrawing groups reacted smoothly, giving isolated products with moderate to high yields between 76% to 95%. Electron-donating aromatic aldehydes (*e.g.*, –Me, –OMe, –OH) were also screened; however, no desired product formation was observed, likely due to reduced electrophilicity of the carbonyl group. Therefore, the study was restricted to electron-withdrawing aromatic aldehydes, which afforded high yields. The range of substrate used is detailed in Table 2.

As an example, the synthesis of compound **4a** was confirmed by seeing a signal singlet at 5.37 ppm in the ^{1}H-NMR spectrum. The key points were that there were no signals for the methylene protons from the 1,3-diethylthiobarbituric acid and no signal for aldehyde proton. Also, the lack of a signal for the aldehyde carbon at 200 ppm in the ^{13}C-NMR spectrum helped to prove that the compound was formed.

In our recycling experiments, a model reaction was used to assess the catalytic performance of [BMIM]OAc. After confirming reaction completion *via* TLC, 5 mL of distilled water was added to precipitate the product, which was then collected by filtration. To recover the catalyst and eliminate water, the filtrate was concentrated under reduced pressure using rotary evaporator at 70–80 °C. this process was carried out for three additional cycles using the recover catalyst. A comparison between the third and the initial run indicated a decrease in product yield, as shown in Fig. 2.

3.2 Biological outcomes

3.2.1 Antimicrobial activity. The antimicrobial activity of compounds **4(a–l)** was evaluated against Gram-positive (*S. aureus*, *B. subtilis*), Gram-negative (*E. coli*), and fungal strains (*C. albicans*, *A. niger*) (Table 3). Compounds **4c** and **4e** showed the highest activity against *S. aureus* (MIC: 8 μg mL^{-1}), more potent than tetracycline (36 μg mL^{-1}) and chloramphenicol (38.8 μg mL^{-1}), and also active against *B. subtilis* (MIC: 16 μg mL^{-1}). Against *E. coli*, **4a**, **4b** and **4f** exhibited the strongest inhibition (MIC: 8 μg mL^{-1}), outperforming the standards, while **4i**, **4j**, and **4k** were less effective (MIC: 64–128 μg mL^{-1}). In antifungal tests, **4l** showed excellent activity against *C. albicans* (MIC: 8 μg mL^{-1}), significantly better than fluconazole (64 μg mL^{-1}) and miconazole (126 μg mL^{-1}), whereas **4c**, **4e**, **4d**, and **4f** had moderate effects (MIC: 32 μg mL^{-1}). Most compounds displayed moderate inhibition against *A. niger* (MIC: 64 μg mL^{-1}), with **4a** and **4g** being weaker (128 μg mL^{-1}). Overall, **4a**, **4b**, **4c**, **4e**, **4f**, and **4l** emerged as the most promising candidates for further antimicrobial development.

3.2.2 Cytotoxicity (MTT assay). Cytotoxic evaluation on HEK-293 cells showed low toxicity for most compounds, with IC_{50} values > 50 μM for the majority of derivatives. Halogenated

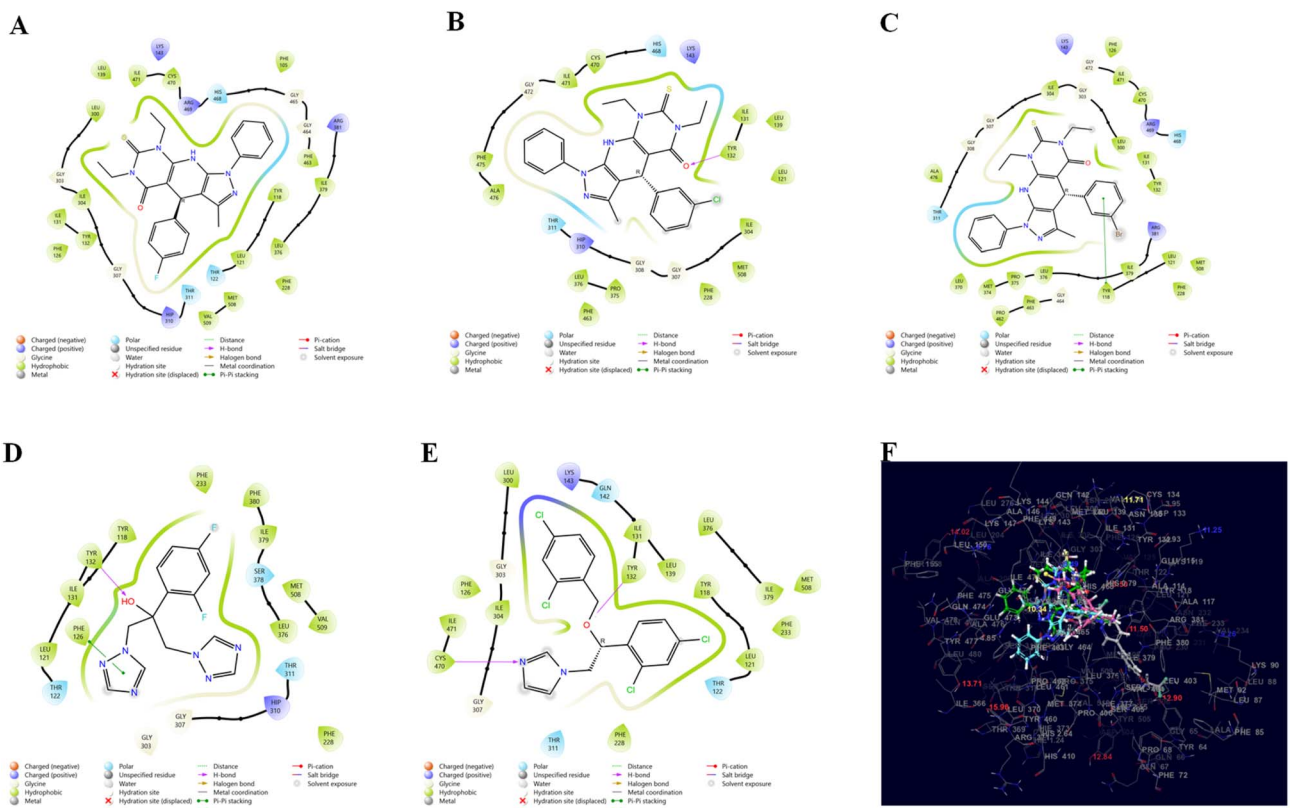

Fig. 4 2D interactions of (A) **4c**, (B) **4e**, (C) **4f**, (D) fluconazole, and (E) miconazole with the crystallized structure of sterol 14-alpha demethylase (PDB ID: 5TZ1). (F) **4c**, **4e**, **4f**, and standard drugs fluconazole and miconazole were superimposed in the VT1 (co-crystallized ligand) binding site of the target (PDB ID: 5TZ1).

analogues (**4c**, **4e**) showed moderate cytotoxicity (IC_{50} ~ 40–50 μM) but remained significantly less toxic than doxorubicin (IC_{50} = 5 μM). Results are presented in Table 4.

The anticancer activity of compounds **4(a–l)** was evaluated using the MTT assay, and the IC_{50} values are summarized in Table 4. Among the tested derivatives, **4e** (42 ± 1.9 μM) and **4c** (45 ± 2.1 μM) exhibited the highest cytotoxic activity, followed closely by **4j** (50 ± 2.3 μM). Other compounds, including **4b**, **4d**, **4f**, and **4h**, displayed moderate activity with IC_{50} values ranging from 55–65 μM, whereas **4a** and **4i** were comparatively less potent (IC_{50} > 100 μM). In comparison, the standard drug doxorubicin showed a markedly higher potency with an IC_{50} of 5 ± 0.4 μM, highlighting its superior cytotoxic effect. Importantly, cytotoxic evaluation against HEK 293 normal human kidney cells revealed that most compounds exhibited low toxicity (IC_{50} > 50 μM), suggesting a favorable safety margin. Notably, halogenated analogues such as **4c** and **4e** demonstrated moderate cytotoxicity (~40–50 μM) but remained significantly less toxic than doxorubicin, underscoring their potential as selective anticancer leads.

3.3 Molecular docking

In case of the molecular docking against the bacterial target, the results showed that the compounds **4c**, **4e**, and **4f** possessed moderate binding affinities towards Tet repressor class D (PDB ID: 2VKE) with Glidescores of −4.378, −4.672, and −4.704 kcal mol^{-1} (Fig. 3(A)–(C), respectively), compared to tetracycline (co-crystallized ligand) at −5.108 kcal mol^{-1} (Fig. 3(D)). All three of **4c**, **4e**, and **4f** showed a common H-bond interaction with the Hie100 (deprotonated form of His) residue (Table 5). Also, these compounds and tetracycline showed mutual polar contacts with Hie100, Gln109, Gln116, Ser138, and Hie139. Additionally, these three compounds showed common hydrophobic interactions with Leu60, Phe86, Pro105, Val113, Ile134, and Leu142 residues. All three compounds, as well as tetracycline, superimposed very well inside the binding pocket of Tet repressor class D.

In case of the molecular docking against the fungal target, the results showed that the compounds **4c**, **4e**, and **4f** possessed moderate binding affinities towards sterol 14-alpha demethylase (PDB ID: 5TZ1) with Glidescores of −7.627, −7.985, and −6.969 kcal mol^{-1} (Fig. 4(A)–(C), respectively), compared to the standard drugs, *i.e.*, fluconazole and miconazole, at −7.589 and −9.792 kcal mol^{-1} (Fig. 4(D) and (E), respectively). Among the three compounds, **4e** showed a mutual H-bond interaction with Tyr132 with both the standard drugs (Table 5). Also, all three compounds showed a common polar contact with Thr311 and His468, while all of them possessed a single mutual polar

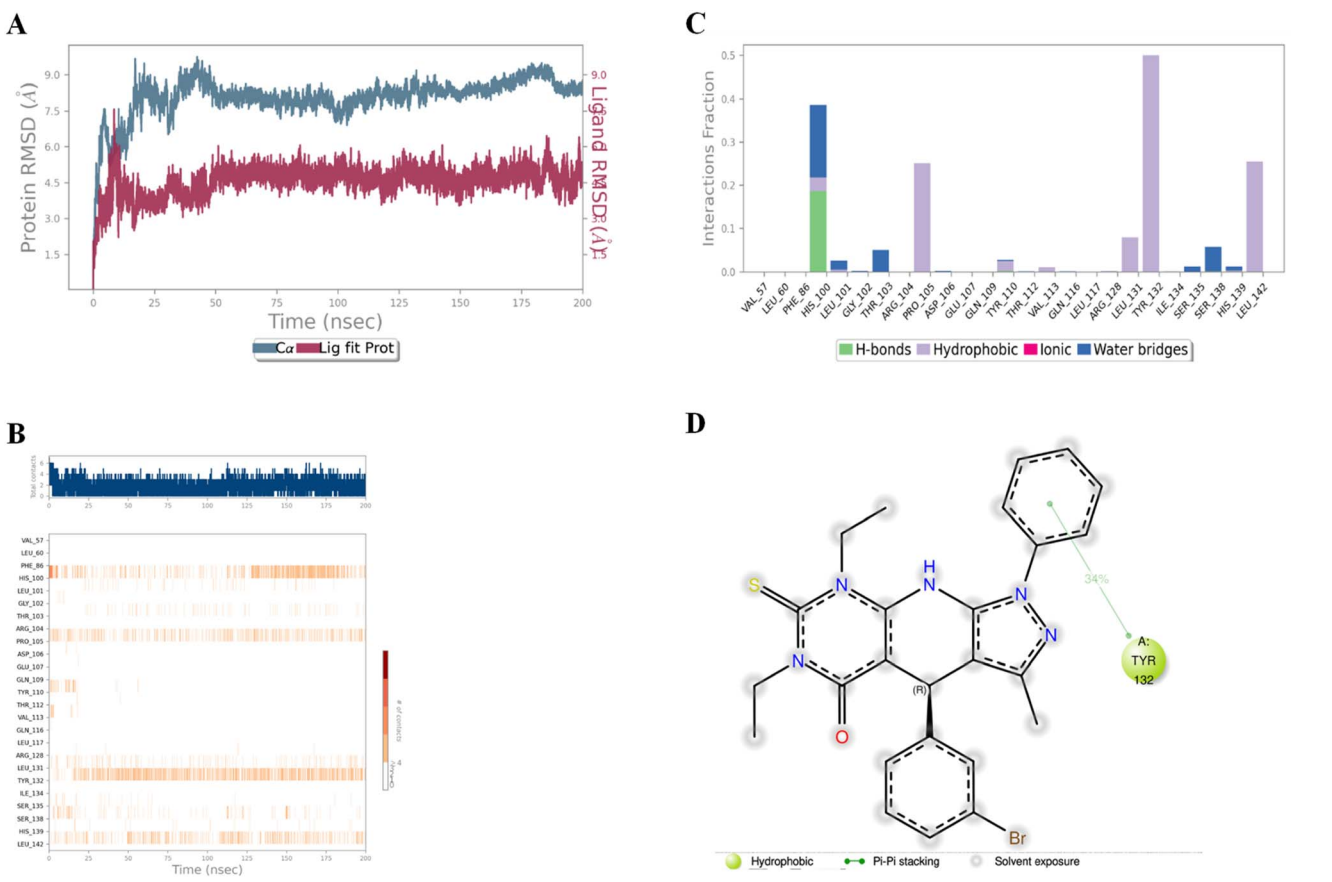

Fig. 5 The results of the molecular dynamics simulations of **4f**-Tet repressor class D-tetracycline (PDB ID: 2VKE). (A) RMSD plot of the protein–ligand complex, (B) protein–ligand contacts diagram, (C) stacked bar plot of the fractions of time of the interactions for 200 ns of simulation time. (D) Ligand atom interactions with the protein residues.

contact with Thr311 residue, with the standard drugs. All 5 compounds (**4c**, **4e**, **4f**, and the standard drugs) showed common hydrophobic interactions with Leu121, Ile131, Tyr132, Phe228, and Met508. All three compounds, as well as the standard drugs, superimposed moderately inside the binding pocket of the target.

3.4 Molecular dynamics (MD) simulations

MD studies of the **4f**-Tet repressor class D (PDB ID: 2VKE) complex and **4f**-sterol 14-alpha demethylase (PDB ID: 5TZ1) were done on the top Glide Score-containing complex. For the **4f**-Tet repressor class D complex (PDB ID: 2VKE), the Root Mean Square Deviation (RMSD) remained below 2 Å throughout the 200 ns molecular dynamics simulation (Fig. 5(A)), indicating moderate structural stability within the tetracycline-binding site of the Tet repressor class D. Analysis of the protein–ligand interaction diagram revealed that His100, Pro105, Tyr132, and Leu142 contribute significantly to complex stability (Fig. 5(B) and (C)). Among these, Pro105, Tyr132, and Leu142 predominantly participate in hydrophobic interactions at the active site, each with an interaction fraction exceeding 0.25. Furthermore, His100 primarily forms hydrogen bonds and water bridges, both persisting for more than 15% of the simulation time. Overall, the *in silico* results suggest that His100, Pro105, and Leu142 are key residues influencing antibacterial activity, consistent with their involvement in the molecular docking interactions of the standard tetracycline compound.

For the **4e**-sterol 14-alpha demethylase complex (PDB ID: 5TZ1), the Root Mean Square Deviation (RMSD) remained below 1 Å during the 200 ns molecular dynamics simulation (Fig. 6(A)), indicating a highly stable complex within the tetrazole-based antifungal binding site of sterol 14-alpha demethylase. According to the protein–ligand interaction analysis, Tyr132, Phe463, His468, and Ala476 play key roles in maintaining the stability of the complex (Fig. 6(B) and (C)). Among these, Phe463 and Ala476 primarily form hydrophobic interactions at the active site, each with an interaction fraction exceeding 0.5. Additionally, Tyr132 and His468 contribute major water–bridge interactions, persisting for more than 60% of the simulation time. There is no significant H-bond interaction (only Thr311; interaction fraction of <0.1) reported here. The conformational stability of the docked complexes was further assessed using MD simulations. Representative snapshots at different simulation time points are shown in Fig. 7.

According to the *in silico* findings, Tyr132 and Leu376 appear to play crucial roles in antifungal activity, as these interactions were consistently observed in the molecular docking results for the reference compounds Fluconazole and Miconazole.

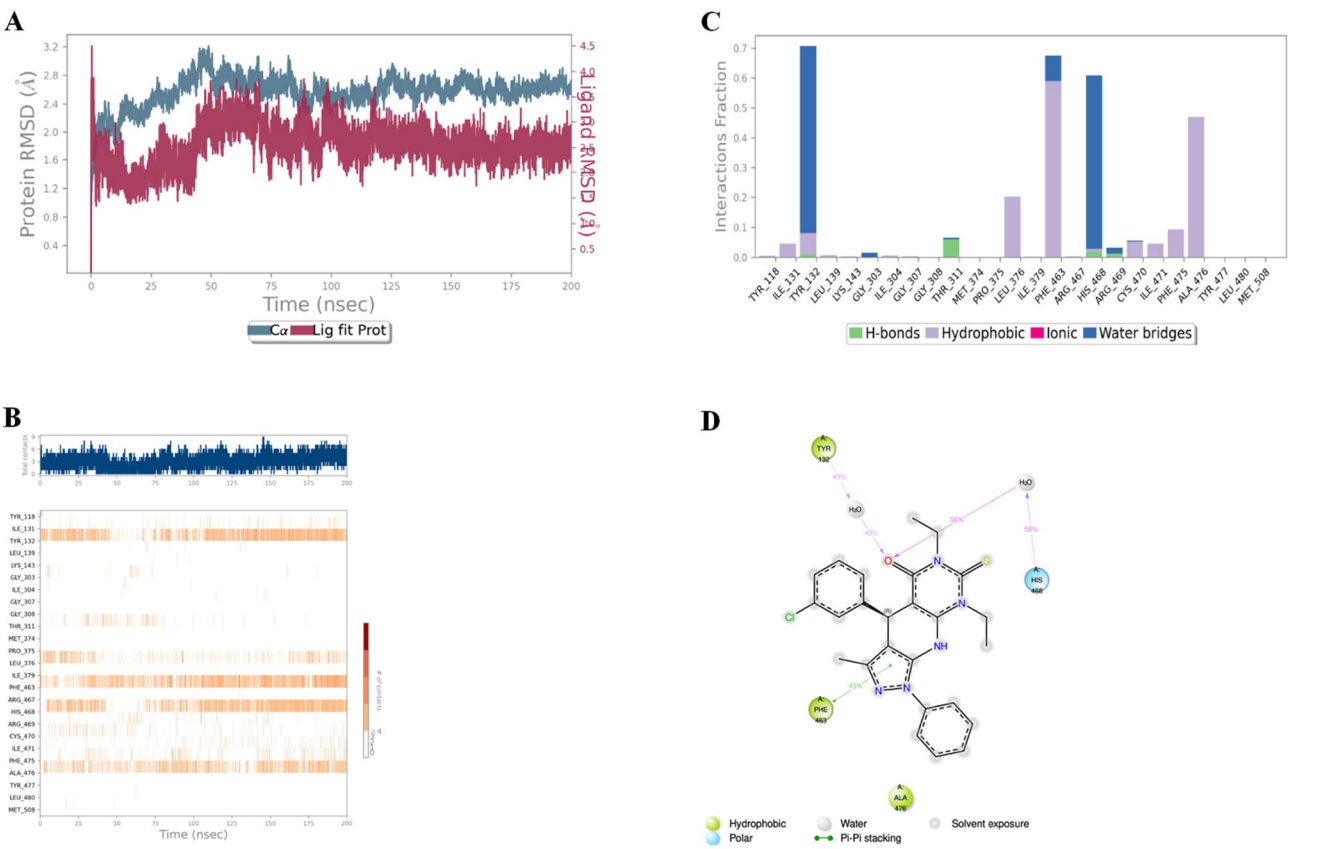

Fig. 6 The results of MD simulations of **4e**-sterol 14-alpha demethylase (PDB ID: 5TZ1) complex. (A) RMSD plot of the 5TZ1-**4e** complex, (B) 5TZ1-4e contacts diagram, (C) stacked bar chart illustrating the interaction fractions over the 200 ns simulation period. (D) Ligand atom interactions with the protein residues.

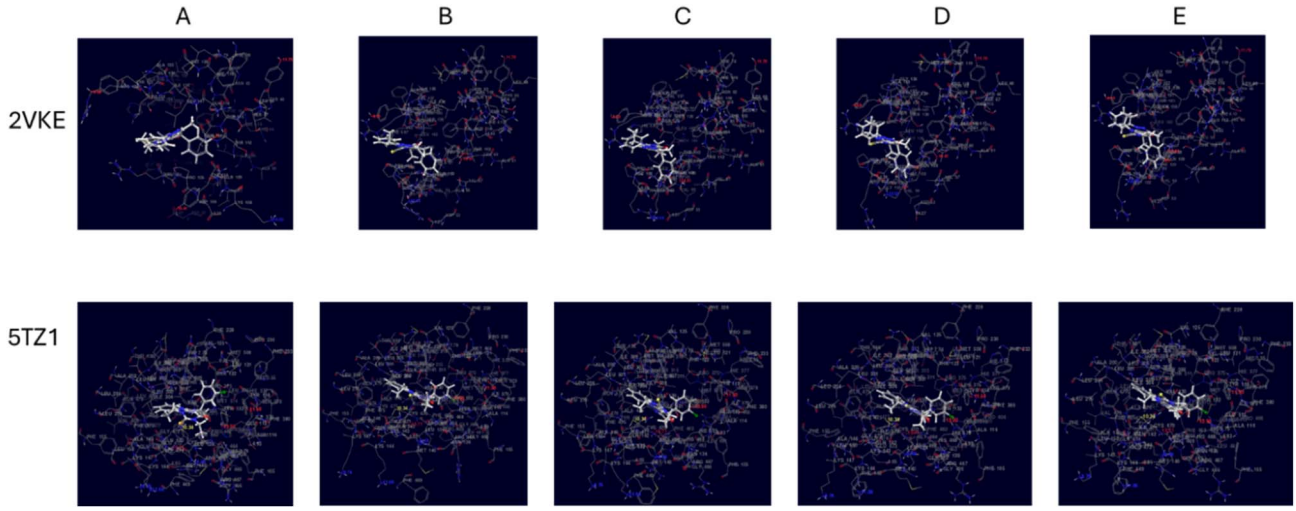

Fig. 7 Results of MD simulations of **4f**-2VKE and **4e**-5TZ1 at 1st (A), 2500th (B), 5000th (C), 7500th (D), 10002nd (E) frames of MD simulations.

4 Conclusion

In summary, we have established a green, efficient, and recyclable ionic-liquid-mediated multicomponent strategy for the synthesis of pyrazolo[4′,3′:5,6]pyrido[2,3-*d*]pyrimidin-5-one derivatives using [BMIM]OAc as a catalyst. This protocol provides several advantages over previously reported methods, including mild reaction conditions, shorter reaction times, excellent product yields, and simple catalyst recovery and reusability, thereby aligning closely with green chemistry principles. The antimicrobial screening studies revealed that compounds **4a**, **4b**, **4c**, **4e**, **4f**, and **4l** exhibited potent activity, outperforming standard reference drugs in selected microorganisms, while the majority of synthesized molecules demonstrated low cytotoxicity, indicating a favourable therapeutic window. Furthermore, molecular docking and MD simulations confirmed strong and stable binding interactions, supporting their biological potential. Overall, this research provides a valuable foundation for future applications of ionic-liquid-assisted multicomponent reactions in medicinal chemistry and supports the further exploration of these heterocycles for potential antimicrobial and anticancer therapeutic development.

Author contributions

Savan S. Bhalodiya: method development, investigation, validation, spectral analysis, writing an original draft, Mehul P. Parmar: writing – review editing, spectral analysis, Shana Balachandran: investigation, biological study, writing – review & editing, formal analysis, Chirag D. Patel: writing – review & editing, formal analysis, Arijit Nandi: computational study, writing – review & editing, visualization, formal analysis, Anwesha Das: computational study, writing – review & editing, formal analysis, Madan Kumar Arumugam: biological study, writing – review & editing, formal analysis, Hitendra M. Patel: writing – review & editing, supervision, method development, investigation, formal analysis, conceptualization.

Conflicts of interest

The authors declare no conflict of interest.

Data availability

The data supporting this article has been included as part of the supporting information (SI). Supplementary information is available. See DOI: https://doi.org/10.1039/d5ra09581f.

Acknowledgements

We would like to extend our heartfelt gratitude to the Department of Chemistry, Sardar Patel University, Vallabh Vidyanagar for providing us with the necessary research facilities. SSB is thankful to the CSIR-NET fellowship (Reference No. Nov/06/2020(i)EU-V). MPP is thankful to the Knowledge Consortium of Gujarat for SHODH fellowship (Student Reference No. 2021016434). CDP is thankful to National fellowship for scheduled Tribe (Award No. 202223-NFST-GUJ-00003). This work was supported by resources provided by The University of Queensland Research Computing Centre's Bunya supercomputer, with funding from The University of Queensland, Brisbane, Australia.

References

1 E. Kabir and M. Uzzaman, *Results Chem.*, 2022, **4**, 100606.
2 H. D. Nguyen and M.-S. Kim, *Comput. Biol. Chem.*, 2023, **104**, 107872.
3 S. Chigurupati, A. Al-murikhy, S. A. Almahmoud, Y. Almoshari, A. Saber Ahmed, S. Vijayabalan, S. Ghazi Felemban and V. Raj Palanimuthu, *Saudi J. Biol. Sci.*, 2022, **29**, 854–859.

4 P. J. Patel, S. G. Patel, D. B. Upadhyay, L. Ravi, A. Dhanasekaran and H. M. Patel, *RSC Adv.*, 2023, **13**, 24466–24473.
5 A. P. Taylor, R. P. Robinson, Y. M. Fobian, D. C. Blakemore, L. H. Jones and O. Fadeyi, *Org. Biomol. Chem.*, 2016, **14**, 6611–6637.
6 K. R. A. Abdellatif and R. B. Bakr, *Med. Chem. Res.*, 2021, **30**, 31–49.
7 S. Schenone, M. Radi, F. Musumeci, C. Brullo and M. Botta, *Chem. Rev.*, 2014, **114**, 7189–7238.
8 K. Kandhasamy, R. R. Surajambika and P. K. Velayudham, *Med. Chem.*, 2024, **20**(3), 293–310.
9 S. S. Bhalodiya, M. P. Parmar, D. B. Upadhyay, C. D. Patel, D. P. Vala, D. Rajani and H. M. Patel, *Results Chem.*, 2024, **7**, 101304.
10 M. P. Parmar, D. P. Vala, S. S. Bhalodiya, D. B. Upadhyay, C. D. Patel, S. G. Patel, S. R. Gandholi, A. H. Shaik, A. D. Miller, J. Nogales, S. Banerjee, J. M. Padrón, N. Amri, N. K. Kandukuri and H. M. Patel, *RSC Adv.*, 2024, **14**, 9300–9313.
11 S. G. Patel, D. B. Upadhyay, N. V. Shah, M. P. Parmar, P. J. Patel, A. Malik, R. K. Sharma and H. M. Patel, *RSC Sustain.*, 2024, **2**, 1128–1141.
12 P. J. Patel, R. M. Vala, S. G. Patel, D. B. Upadhyay, D. P. Rajani, F. Damiri, M. Berrada and H. M. Patel, *J. Mol. Struct.*, 2023, **1285**, 135467.
13 R. Javahershenas, J. Han, M. Kazemi and P. J. Jervis, *ChemistrySelect*, 2024, **9**, e202401496.
14 M. P. Parmar, S. Kashyap, D. P. Vala, S. S. Bhalodiya, C. D. Patel, J. Nogales, A. Nandi, S. Banerjee and H. M. Patel, *Eur. J. Med. Chem.*, 2025, **297**, 117914.
15 D. M. Patel, P. J. Patel and H. M. Patel, *Eur. J. Org Chem.*, 2022, **2022**, e202201119.
16 R. Javahershenas, J. Han, M. Kazemi and P. J. Jervis, *ChemistryOpen*, 2024, **13**, e202400185.
17 R. Javahershenas and S. Nikzat, *RSC Adv.*, 2023, **13**, 16619–16629.
18 S. S. Bhalodiya, M. P. Parmar, C. D. Patel, S. G. Patel, D. P. Vala, N. Suresh, B. Jayachandran, M. Kumar Arumugam, M. Narayan and H. M. Patel, *ChemMedChem*, 2025, **20**, e202400595.
19 M. P. Parmar, A. Das, D. P. Vala, S. S. Bhalodiya, C. D. Patel, S. Balachandran, N. K. Kandukuri, S. Kashyap, A. N. Khan, A. González-Bakker, M. K. Arumugam, J. M. Padrón, A. Nandi, S. Banerjee and H. M. Patel, *ACS Omega*, 2025, **10**, 7013–7026.
20 D. B. Upadhyay, J. A. Mokariya, P. J. Patel, S. G. Patel, A. Das, A. Nandi, J. Nogales, N. More, A. Kumar, D. P. Rajani, M. Narayan, J. Kumar, S. Banerjee, S. K. Sahoo and H. M. Patel, *Arch. Pharmazie*, 2024, **357**, 2300673.
21 M. A. P. Martins, C. P. Frizzo, D. N. Moreira, N. Zanatta and H. G. Bonacorso, *Chem. Rev.*, 2008, **108**, 2015–2050.
22 N. Isambert, M. d. M. S. Duque, J.-C. Plaquevent, Y. Génisson, J. Rodriguez and T. Constantieux, *Chem. Soc. Rev.*, 2011, **40**, 1347–1357.
23 S. Rajamanickam and B. Dam, in *Handbook of Ionic Liquids*, 2024, pp. 419–442, DOI: 10.1002/9783527839520.ch21.
24 M. Zakeri, M. M. Nasef and E. Abouzari-Lotf, *J. Mol. Liq.*, 2014, **199**, 267–274.
25 J. B. Bharate, S. B. Bharate and R. A. Vishwakarma, *ACS Comb. Sci.*, 2014, **16**, 624–630.
26 F. Shirini, M. S. N. Langarudi, N. Daneshvar, M. Mashhadinezhad and N. Nabinia, *J. Mol. Liq.*, 2017, **243**, 302–312.
27 O. G. Jolodar, F. Shirini and M. Seddighi, *Chin. J. Catal.*, 2017, **38**, 1245–1251.
28 A. Arias-Gómez, A. Godoy and J. Portilla, *Molecules*, 2021, **26**(9), 2708.
29 P. Yadav and K. Shah, *Chemical Biology & Drug Design*, 2021, vol. 97, pp. 633–648.
30 D. J. Baillache and A. Unciti-Broceta, *RSC Med. Chem.*, 2020, **11**, 1112–1135.
31 A. Ballesteros-Casallas, M. Paulino, P. Vidossich, C. Melo, E. Jiménez, J.-C. Castillo, J. Portilla and G. P. Miscione, *Eur. J. Med. Chem. Rep.*, 2022, **4**, 100028.
32 H. C. Patel, M. S. Patel, J. N. Parekh, D. D. Chudasama, P. Dalwadi, A. Kunjadiya, V. Bhatt, K. M. Modi, C. N. Patel and K. R. Ram, *J. Biomol. Struct. Dyn.*, 2025, **43**, 3467–3490.
33 A. S. Hassan, N. M. Morsy, H. M. Awad and A. Ragab, *J. Iran. Chem. Soc.*, 2022, **19**, 521–545.
34 E. H. El-Sayed and K. S. Mohamed, *Polycyclic Aromat. Compd.*, 2021, **41**, 1077–1093.
35 S. Deshmukh, K. Dingore, V. Gaikwad and M. Jachak, *J. Chem. Sci.*, 2016, **128**, 1459–1468.
36 M. Faisal, A. Saeed, S. Hussain, P. Dar and F. A. Larik, *J. Chem. Sci.*, 2019, **131**, 70.
37 N. Abbas, P. M. G. Swamy, P. Dhiwar, S. Patel and D. Giles, *Pharm. Chem. J.*, 2021, **54**, 1215–1226.
38 G. Rajitha, V. Ravibabu, G. Ramesh and B. Rajitha, *Res. Chem. Intermed.*, 2016, **42**, 1989–1998.
39 P. Rathee, R. Tonk, A. Dalal, M. Ruhil and A. Kumar, *Cell. Mol. Biol.*, 2016, **62**, 4172.
40 A. K. Oraby, R. Khaled, M. Abdelgawad, K. Attia and P. Georghiou, *Int. J. Pharm. Chem.*, 2016, **6**, 100–106.
41 A. Bazgir, M. M. Khanaposhtani and A. A. Soorki, *Bioorg. Med. Chem. Lett.*, 2008, **18**, 5800–5803.
42 S. P. Satasia, P. N. Kalaria and D. K. Raval, *Org. Biomol. Chem.*, 2014, **12**, 1751–1758.
43 M. Daraie, M. M. Heravi, M. Mirzaei and N. Lotfian, *Appl. Organomet. Chem.*, 2019, **33**, e5058.
44 M. A. Ghasemzadeh, B. Mirhosseini-Eshkevari and S. Sanaei-Rad, *Polyhedron*, 2022, **212**, 115588.
45 M. M. Heravi and M. Daraie, *Molecules*, 2016, **21**(4), 441.
46 M. Daraie and M. M. Heravi, *Arkivoc*, 2016, **2016**, 328–338.
47 Y. K. Mahdi, M. R, D. Kumar, A. Nandi, A. Das, Y. A. Atia, R. Ranjan and Y. N. Dey, *Curr. Trends Biotechnol. Pharm.*, 2023, **17**, 1496–1505.
48 K. J. Bowers, E. Chow, H. Xu, R. O. Dror, M. P. Eastwood, B. A. Gregersen, J. L. Klepeis, I. Kolossvary, M. A. Moraes, F. D. Sacerdoti, J. K. Salmon, Y. Shan and D. E. Shaw, *Presented in Part at the Proceedings of the 2006 ACM/IEEE Conference on Supercomputing*, Tampa, Florida, 2006.
49 A. Nandi, N. Mandal, A. Das and Y. N. Dey, *J. Biol. Regul. Homeostatic Agents*, 2024, **38**, 2055–2067.